

ARTICLE

Open Access

# Wide field of view large aperture meta-doublet eyepiece

Anna Wirth-Singh<sup>1✉</sup>, Johannes E. Frösch<sup>1,2</sup>, Fan Yang<sup>3</sup>, Louis Martin<sup>3</sup>, Hanyu Zheng<sup>3</sup>, Hualiang Zhang<sup>4</sup>, Quentin T. Tanguy<sup>2</sup>, Zhihao Zhou<sup>2</sup>, Luocheng Huang<sup>2</sup>, Demis D. John<sup>5</sup>, Biljana Stamenic<sup>5</sup>, Juejun Hu<sup>3</sup>, Tian Gu<sup>3</sup> and Arka Majumdar<sup>1,2✉</sup>

## Abstract

Wide field of view and light weight optics are critical for advanced eyewear, with applications in augmented/virtual reality and night vision. Conventional refractive lenses are often stacked to correct aberrations at a wide field of view, leading to limited performance and increased size and weight. In particular, simultaneously achieving a wide field of view and large aperture for light collection is desirable but challenging to realize in a compact form-factor. Here, we demonstrate a wide field of view (greater than 60°) meta-optic doublet eyepiece with an entrance aperture of 2.1 cm. At the design wavelength of 633 nm, the meta-optic doublet achieves comparable performance to a refractive lens-based eyepiece system. This meta-doublet eyepiece illustrates the potential for meta-optics to play an important role in the development of high-quality monochrome near-eye displays and night vision systems.

## Introduction

Alongside advances in artificial intelligence and widespread availability of digital content, demand for augmented reality (AR) and virtual reality (VR) near-eye displays has surged. There is great commercial interest in developing such technologies for education, gaming, and social interactions, and also significant defense and national security interest for night vision and enhanced vision. The human eye is a highly optimized system, so exceptional optical performance is required to facilitate the interaction between the user and virtual reality. For reference, human vision's full field of view is approximately 120°<sup>1</sup>, which exceeds the performance of most "wide" (generally > 60°) angle camera systems. However, achieving such performance in near-eye displays presents significant optical engineering challenges<sup>2,3</sup>. In addition, near-eye optics must be thin and lightweight for user comfort and safety, especially for long-duration usage to reduce fatigue. With traditional optics, there is often a

trade-off between compact form factor and performance, and the ultimate challenge of near-eye displays is that it demands both.

A comfortable reading distance is around 35 cm<sup>4</sup>, which is much greater than the distance between a head-mounted near-eye display and the eye. The challenge for near-eye optics, then, is to project the image on a display that is placed close to the eye to a comfortable viewing distance to avoid visual fatigue and discomfort<sup>3,5,6</sup>. Similarly, a common configuration for night vision goggles is to collect reflected nightglow in the near infrared via an objective lens, intensify and upconvert that light to monochromatic visible illumination via intensifier tubes, and couple that light into the eye via an eyepiece optics<sup>7</sup>. In both applications, eyepiece optics are required to collimate near-eye illumination in order to project the image to a comfortable viewing distance. It is desirable to mount such optics near the head to minimize torque on the wearer and maintain a compact form factor; on the other hand, the minimum acceptable physical distance between an optic and the surface of the eye (called eye relief) is about 1.5 cm. This provides a small amount of working space, thus requiring compact optics. Pancake optics are commonly used, but suffer from low efficiency due to polarization conversions<sup>8</sup>. Several emerging optical

Correspondence: Anna Wirth-Singh ([annaw77@uw.edu](mailto:annaw77@uw.edu)) or Arka Majumdar ([arka@uw.edu](mailto:arka@uw.edu))

<sup>1</sup>Department of Physics, University of Washington, Seattle, WA, USA

<sup>2</sup>Department of Electrical and Computer Engineering, University of Washington, Seattle, WA, USA

Full list of author information is available at the end of the article

© The Author(s) 2025



**Open Access** This article is licensed under a Creative Commons Attribution 4.0 International License, which permits use, sharing, adaptation, distribution and reproduction in any medium or format, as long as you give appropriate credit to the original author(s) and the source, provide a link to the Creative Commons licence, and indicate if changes were made. The images or other third party material in this article are included in the article's Creative Commons licence, unless indicated otherwise in a credit line to the material. If material is not included in the article's Creative Commons licence and your intended use is not permitted by statutory regulation or exceeds the permitted use, you will need to obtain permission directly from the copyright holder. To view a copy of this licence, visit <http://creativecommons.org/licenses/by/4.0/>.

technologies are poised to meet the demands of near-eye displays, including holographic optical elements<sup>3,9,10</sup> and leaky waveguides<sup>11,12</sup>. Integrating metasurfaces directly onto micro-LED displays for collimation has also been proposed<sup>13</sup> but not yet experimentally demonstrated.

Ultra-thin and versatile meta-optics are another promising platform for near-eye displays. Meta-optics consist of arrays of sub-wavelength scatterers which impart spatially-varying phase shifts to incident light. Thanks to advancements in nanoscale lithography techniques, the fabrication of meta-optics at near-infrared and visible wavelengths is now regularly accomplished, with recent works demonstrating visible and near-infrared meta-optics with wide field of view<sup>14–17</sup>, broadband performance<sup>18–20</sup>, and large aperture<sup>21</sup> for various applications, including AR/VR<sup>22–26</sup>. In particular, the ability to achieve wide field of view in compact form-factor renders meta-optics particularly suitable for near-eye display applications. In singlet meta-optic lenses, nearly diffraction-limited performance has been experimentally demonstrated with over 170° field of view at mid-infrared and near-infrared wavelengths<sup>15</sup>, albeit with a relatively small entrance aperture of 1 mm ( $\approx 200\lambda$ ). In another work, by relaxing the constraint on diffraction-limited performance, Martins et al.<sup>14</sup> demonstrate 178° field of view with larger entrance aperture of 2 mm ( $\approx 3750\lambda$ ).

Similar to traditional refractive optics, stacking several lenses in doublet or triplet configurations provides more degrees of freedom for improved performance and additional functionalities. For example, meta-optic doublets have been used to correct monochromatic aberrations like spherical aberration, coma, and astigmatism as early as 2016 in near-infrared<sup>16</sup> and visible<sup>27</sup> wavelengths by patterning two metasurfaces on two sides of a single transparent substrate. While impressive, both of these designs had entrance apertures less than 1 mm, which is insufficient to be used as an eyepiece for near-eye displays. Since monochromatic Seidel aberrations scale with aperture size and field angle, achieving high optical quality is inherently difficult for simultaneously large aperture and wide field of view optics<sup>28</sup>. In order to achieve diffraction-limited resolution over large field of view and relatively large aperture, it has been shown that doublet configurations are required<sup>29</sup>. In such a configuration, the first metasurface functions as both entrance aperture and a corrective plate, and the second functions a focusing lens.

In this work, we demonstrate high-quality image projection over 60° field of view at 633 nm via a meta-optic doublet for eyepiece applications. To meet the stringent challenges of these applications and simultaneously achieve large aperture and wide field of view within a compact form-factor, we utilize a doublet consisting of two layers of meta-optics. We take a step-by-step approach towards realizing large aperture (2 cm,  $\approx$

31,500 $\lambda$ ) optics by first demonstrating the concept on a 1 cm aperture meta-optic doublet with 80° field of view. We then demonstrate the full-scale system with a large aperture (2 cm) and 60° field of view. The system is designed for realistic eye relief (15 mm), pupil size (5.4 mm), and display size (16 mm). We show excellent experimental agreement with the theoretical model for both sets of optics. Further, compared to a similar commercially available refractive lens eyepiece system, the meta-optic system is superior in terms of improved image quality over wide field of view at the design wavelength and reduced total track length. This work closes the gap between the previous wide field of view metalens demonstrations and practical applications.

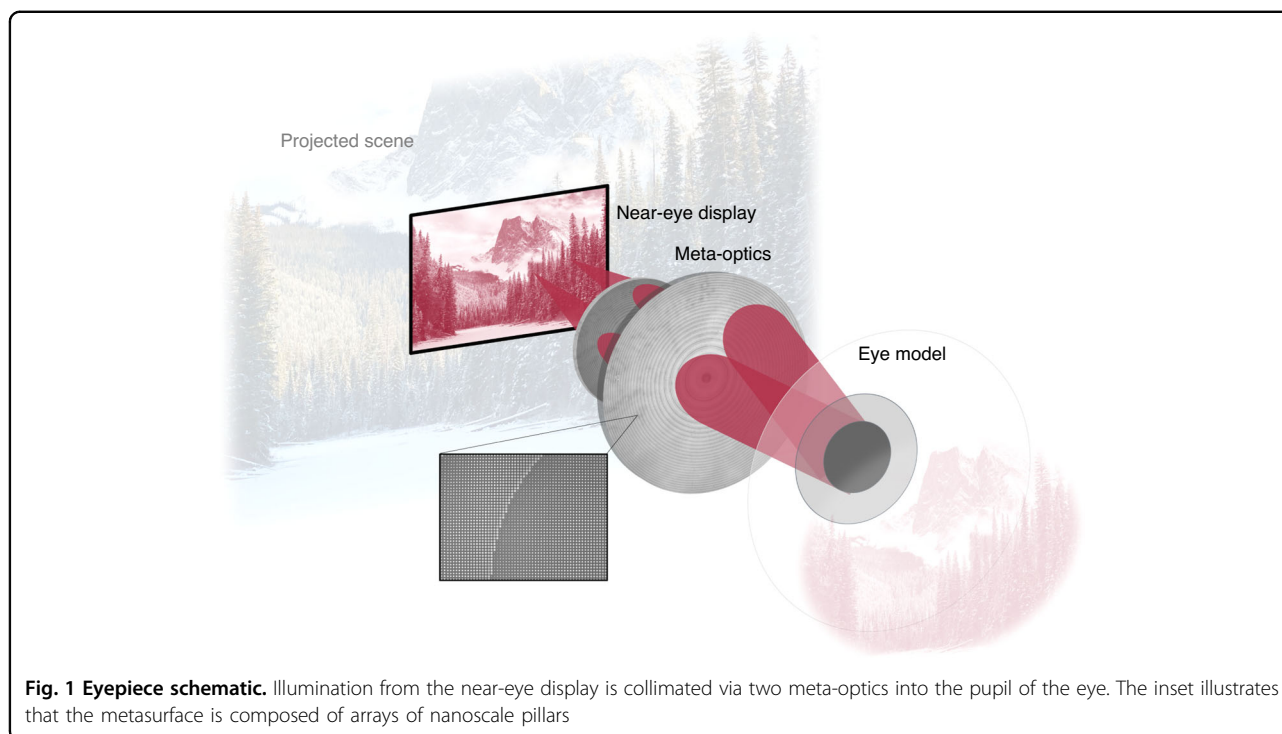
## Results

### Design and modeling

The concept of the wide field of view eyepiece is schematically illustrated in Fig. 1. The meta-optic is designed to collimate light from a near-eye display into the pupil with greater than 60° field of view. When the optics exhibit wide field of view functionality similar to that of the human eye, the user perceives a wide scene comfortably located at infinity, despite the display being physically located near the eye.

In greater detail, ray tracing diagrams of the designed meta-optic doublet systems are shown in Fig. 2. The 1 cm aperture design, shown in Fig. 2a, is demonstrated as a proof of concept prior to the full aperture (2 cm) design shown in Fig. 2b. In both cases, the system consists of a display (at the left), the two meta-optics (labeled MS1 and MS2) mounted on glass spacers with a small air gap in between, and the pupil aperture. Since beams with wide field of view diverge quickly, the required size of MS1 to collect the diverging beams rapidly increases; to mitigate this, optical windows (fused silica ( $n = 1.46$ ) in the 1 cm designs and BK7 glass ( $n = 1.52$ ) in the 2 cm designs) are used to reduce the beam divergence. Similar to other metasurface doublet systems<sup>16,27</sup>, the entrance meta-optic (labeled MS2) functions as both an aperture stop and corrector plate, and the second meta-optic (labeled MS1) possesses the majority of the focusing power. The phase profiles were optimized using Zemax OpticStudio (more details in the Supplementary Information). We designed the system for 80° full field of view in the 1 cm system and 60° full field of view in the 2 cm system; in this case, the field of view is practically limited by the size of the second meta-optic due to fabrication constraints.

As schematically illustrated in Fig. 2c, the meta-optics consist of quasi-periodic arrays of rectangular pillars. To provide full  $2\pi$  phase shift while maintaining high transmission, we use 750 nm tall silicon nitride ( $n = 2.04$ <sup>30</sup>) pillars with widths ranging from 80 to 310 nm on quartz ( $n = 1.46$ <sup>31</sup>) substrate. The lattice periodicity is 350 nm



and the expected transmission is greater than 80% at normal incidence. To determine the corresponding phase delay of the structure, we used rigorous coupled wave analysis (RCWA)<sup>32</sup> to calculate phase shift as a function of pillar width for various angles of incidence, as shown in Fig. 2c. We selected eleven unique unit cell widths to comprise the pillar library, and the calculated phase and transmittance values of those unit cells are provided in Supplementary Table S2. Due to the quasi-periodic nature, the phase shift from individual meta-atoms is not very sensitive to angle of incidence and thus we utilize the normally incident phase-width response to map between pillar width and phase when designing the optics. An analysis of angle-dependent errors is provided in the Supplementary Information. To reduce memory consumption during this mapping, we utilized the circular symmetry of the optic to generate a quarter of the radius width map and then copied and rotated the structure to produce the full circular optics. Some reduction in transmission is expected as the incident angle is increased; the calculated transmission for various angles of incidence is shown in Supplementary Fig. S1b.

For comparison, we include a ray tracing diagram of a similar commercially available refractive lens eyepiece (Edmund Optics 66-210, 21 mm EFL RKE Precision Eyepiece) in Fig. 2d. The refractive system has similar entrance aperture (20 mm) as our 2 cm meta-optic system and slightly longer effective focal length (21 mm for the refractive system versus 15 mm for the meta-optic system).

We present both systems under the same pupil and eye relief conditions, namely 5.4 mm pupil diameter and 15 mm eye relief. From the ray tracing diagram, distortion is evident in the refractive system at wide field of view, whereas the designed meta-optic system exhibits very little distortion, even at incident angles of 30°. In Table 1, we summarize the key design specifications of the discussed systems, including their effective focal length, numerical aperture, total track length, and eye relief. The effective focal length and numerical aperture were calculated from the Zemax model. We show the simulated ray aberration and distortion curves in Supplementary Fig. S3.

#### Meta-optics fabrication and characterization

The meta-optics were fabricated in silicon nitride on quartz using electron beam lithography and inductively coupled plasma (ICP) fluorine etching, with further details in Methods. Optical microscope and scanning electron microscope (SEM) images of the fabricated devices are shown in Fig. 3a, b to highlight the fabrication quality. Some of the larger pillars are not fully separated due to resolution constraints. The silica and glass spacers were obtained from commercial sources (2 mm thick fused silica: Newport FSW14; 8 mm thick BK7 glass: Thorlabs WG11508; 10 mm thick BK7 glass: Newport 20BW40-30).

The fabricated optics, shown next to a ruler for scale, are shown in Fig. 3c. The maximum aperture that we could fabricate using electron beam lithography was approximately 1 cm diameter, limited by the stability of

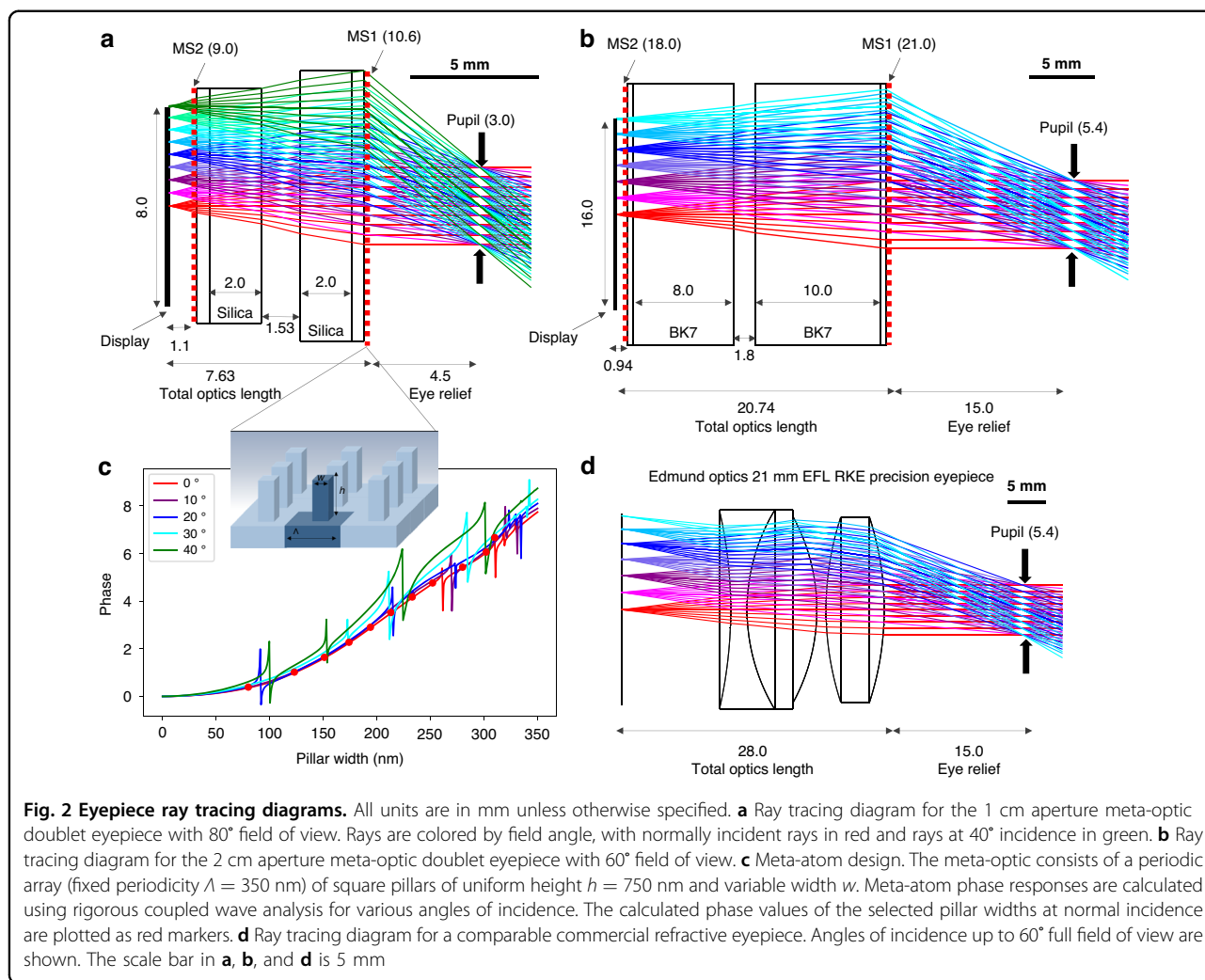


**Table 1 Eyepiece Design Specifications**

	1 cm Meta-Optic Doublet	2 cm Meta-Optic Doublet	Refractive Triplet
Entrance Aperture (mm)	10.6	21.0	20.0
Designed field of view (°)	80	60	45*
Pupil Diameter (mm)	3.0	5.4	5.4
Eye Relief (mm)	4.5	15.0	15.0
Effective Focal Length (mm)	5.84	15.17	21.61
Numerical Aperture	0.25	0.18	0.124
Total Track Length (mm)	12.1	35.7	43.0

\* Reported apparent field of view

the machine over extended write time. Therefore, the 2 cm eyepiece optics require a larger write area than realistically feasible using our methods. To circumvent this issue, we fabricated the entire aperture of the 1 cm meta-

optics and only a slice of the 2 cm optics which was required to characterize the point spread function (PSF) of the optics. To measure the PSF, only the projected area of the pupil aperture (5.4 mm) is illuminated; therefore,

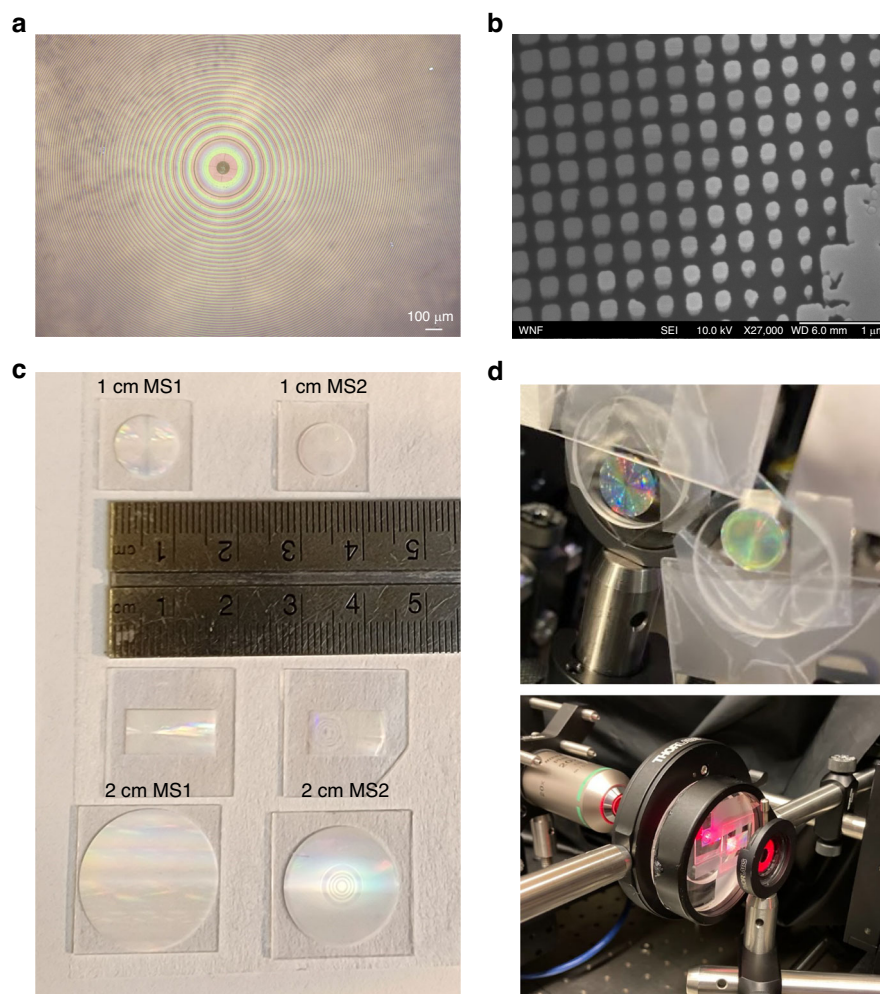
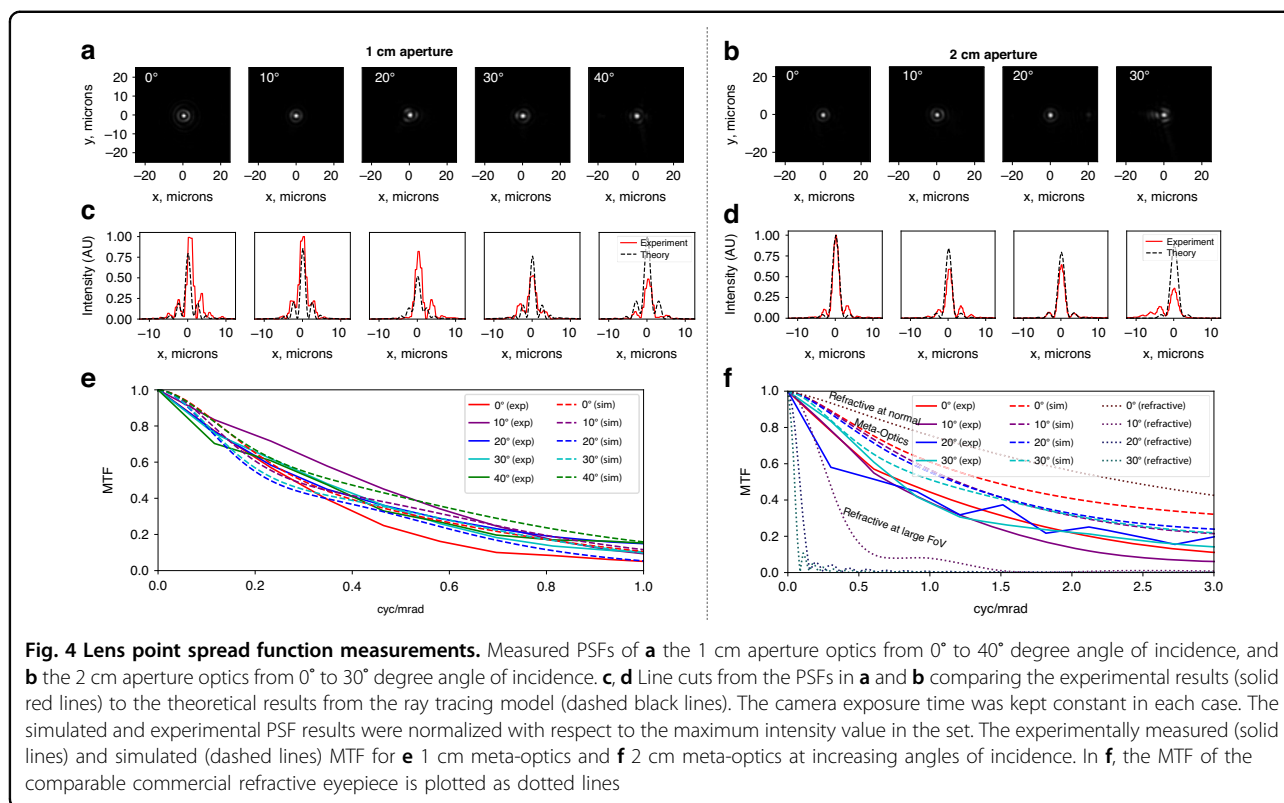


**Fig. 3 Fabricated meta-optics.** **a** Optical microscope image of the fabricated meta-optics. **b** SEM image of the fabricated optics at slightly oblique ( $10^\circ$ ) viewing angle. **c** A photo of all fabricated meta-optics next to a ruler for scale. From top to bottom: the 1 cm aperture meta-optics, the 5.4 mm wide slices of the 2 cm meta-optics, and the full 2 cm aperture meta-optics fabricated using lower resolution scatterers. **d** A photograph of the 1 cm meta-optics (top) and 2 cm meta-optics (bottom) mounted on spacers in the experiment setup

the PSF characterization can be completed using only a slice of the metasurface with a dimension of 5.4 mm by 13.2 mm, covering the center to the outer edge. Therefore, we present PSF measurements of both the 1 cm and 2 cm optics and imaging results for the 1 cm optics only. In addition to electron beam lithography, we further describe fabrication of the full aperture 2 cm optics using deep ultraviolet (DUV) lithography; these optics are pictured at the bottom of Fig. 3c and further details are provided in the Supplementary Information. While DUV lithography is a more scalable lithography process, the resolution of our process was limited to approximately 250 nm which is insufficient for sub-wavelength periodicity. The pictured full aperture 2 cm meta-optics are functional up to approximately  $40^\circ$  full field of view, limited by aliasing issues arising from large periodicity (see the Supplementary Information for details).

In Fig. 3d, we show the fabricated optics in the experimental setup. To evaluate the performance of the fabricated meta-optics, we measured the PSF at various angles of incidence using collimated output from a HeNe laser ( $\lambda = 632.8$  nm, linewidth = 1400 MHz) as the illumination source and an iris as the pupil aperture. The simulated and measured PSFs are summarized in Fig. 4. In both the 1 cm and 2 cm aperture designs, the PSF (Fig. 4a and b, respectively) remains mostly undistorted as the angle of incidence is increased. A horizontal line cut through each PSF is shown below, in Fig. 4c, d, with the simulated PSF overlain in a dashed black line. The PSF width is in close agreement with the theory. For both the 1 cm and 2 cm systems, the PSF is normalized to the maximum measured intensity of that system. Some reduction in PSF intensity at a larger angle of incidence is expected and observed, with the measured PSF intensity at 20 degrees off-axis



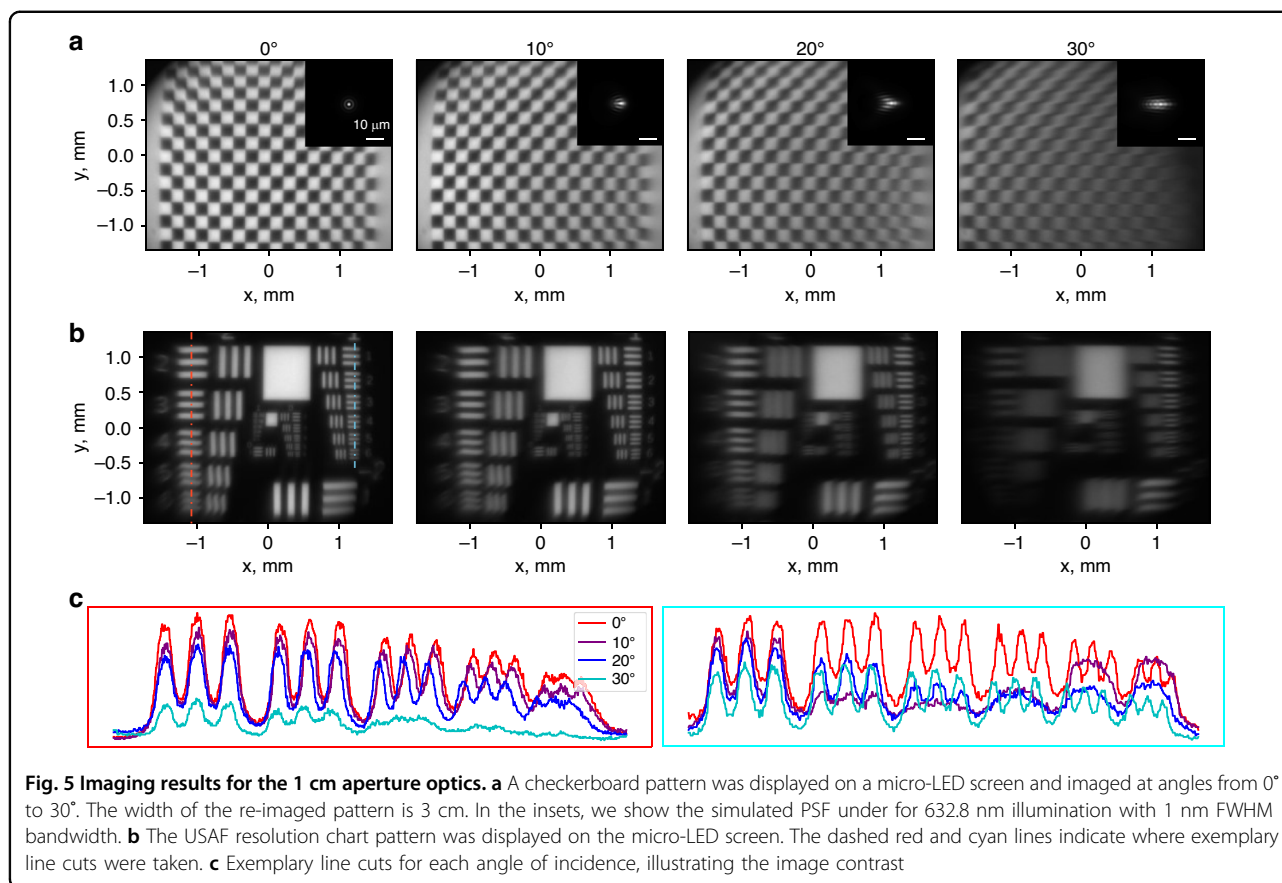
being 82% and 64% of that at normal incidence for the 1 cm and 2 cm designs, respectively. However, the PSF width remains mostly undistorted, highlighting the utility of the lens system over a wide field of view. In addition, the measured transmission through the optics is consistent with that predicted by RCWA (see Supplementary Fig. S1). At normal incidence, the measured transmission through the 1 cm optics were measured to be 70% through MS1 alone, 83% through MS2 alone, and 63% through the system of both optics.

As another measure of optical performance, the modulation transfer function (MTF) describes the image contrast as a function of frequency. For an eyepiece optic with the function of projecting a displayed image to infinity, it is more appropriate to characterize the performance in terms of angular resolution (in cycles/mrad) rather than spatial resolution. From the measured point spread functions, we calculate the MTF at various angles of incidence in Fig. 4e, f. The experiment results (solid lines) show consistent performance over the entire field of view and good agreement with the simulated MTF (dashed lines). While the spatial resolution is similar for the 1 cm and 2 cm optics, the angular resolution of the 2 cm optics is much higher due to its longer effective focal length. For comparison, we plot the simulated MTF of the exemplary commercial refractive system (the same system depicted in Fig. 2d) as darker dotted lines in Fig. 4f. While

the refractive system has higher MTF at normal incidence, it drops rapidly at increasing angles of incidence, showing a true FoV of less than 20 degrees. This is in contrast to the designed meta-optics, which exhibit similar performance across the entire field of view.

In general, the meta-optics experiment results exhibit excellent agreement with the ray tracing simulation. Upon close inspection, it is noted that under some conditions (namely 10° through 30° in the 1 cm optics) the experiment appears to slightly outperform the simulation. However, it should also be noted that the experimental performance is worse than the simulation at normal incidence. Therefore, we attribute the unexpectedly higher experimental performance to be due to slight misalignment which favors slightly off-axis angles. In the case of the 2 cm optics, the simulated results are consistently better than the experiment.

In Fig. 5, we demonstrate the imaging quality of the 1 cm optics over a wide field of view. To demonstrate imaging in a near-eye display configuration, we built an eye model consisting of an iris as the pupil, a refractive lens of 2.5 mm focal length as the eye's lens, and the camera sensor. The lens and camera sensor were mounted on a rotating arm to capture images at wide field of view. To create the imaging object, we displayed an image on a micro-LED display and re-imaged the pattern using a high NA objective (Nikon Plan Fluorite 20x) followed by a



633 nm narrowband filter (Thorlabs FLH632.8-1, FWHM 1 nm). After passing through the objective, the size of the imaging object was approximately 3 mm wide. The displayed pattern was a checkerboard in Fig. 5a and a USAF resolution chart in Fig. 5b. The display, filter, and objective were mounted on a stage and translated laterally to cover the designed display size and demonstrate imaging over 60° full field of view. In the insets in Fig. 5c, we show exemplary line cuts through the red (left) and cyan (right) dashed lines to illustrate image contrast. Due to the slightly broad linewidth of the illumination source (FWHM 1 nm), the resolution is negatively affected by chromatic aberrations. In particular, off-axis performance is negatively affected by chromatic aberrations as the meta-optic phase gradient disperses illumination of different wavelengths. To elucidate this effect, we plot simulated polychromatic PSFs in the insets to Fig. 5a. These PSFs were simulated for 20 wavelengths between 630.5 nm and 635.0 nm, appropriately weighted to match the transmission spectrum of the narrowband filter. Lateral distortion of the PSF is apparent and worsens at increasing angle of incidence. We also note that some reduction in image quality can be attributed to the unit cell's reduced transmission at larger angles of incidence. Nonetheless, we demonstrate high-quality imaging up to

30° angle of incidence corresponding to 60° full field of view.

## Discussion

In this work, we balance trade-offs between compact form factor, aperture size, and field of view to achieve performance in a meta-optical doublet that is comparable to a commercial refractive eyepiece and meets common benchmarks of near eye displays. We note that the performance of the meta-optic doublet is not diffraction-limited, but diffraction-limited performance is typically not required for direct view applications, including AR/VR or night vision. In particular, human visual acuity of 20/20 corresponds to 1 arcmin angular resolution<sup>2</sup>, or about 0.3 mrad. At this resolution, the contrast achieved with the meta-optic eyepiece is approximately 50%, which is sufficient to resolve most features. As shown in Fig. 4f, the imaging quality is comparable to that of a similar commercial refractive lens at normal incidence and better at wide field of view. While the field of view demonstrated in the meta-optic eyepiece is wide relative to many camera lenses, extending the field of view further to a minimum of 100° is desirable for a truly immersive AR/VR experience<sup>3,33</sup>.

The specifications of 80° field of view for the 1 cm optics and 60° field of view for the 2 cm optics were chosen

considering the tradeoffs between form-factor, aperture size, and field of view. In this work, the primary limitation on the field of view is the maximum diameter of meta-optics which can be reasonably fabricated. By increasing the diameter of MS1, the meta-optic can capture light at larger angles of incidence, which would increase the attainable field of view. As shown in several works, meta-optics achieving nearly 180° field of view have been demonstrated, but only for small entrance aperture<sup>14,15</sup>. In fact, it has been shown that in order to simultaneously achieve large aperture and diffraction-limited performance over wide field of view, it is necessary to increase the thickness of the optical system<sup>29,34,35</sup>. Intuitively, this occurs because light of different angles of incidence must be spatially separated, which is easily achieved using a small entrance aperture to restrict light of different angles to interact with different sections of the lens. On the other hand, light at large angles of incidence diverges quickly if the meta-optics are separated by an air gap, and this introduces two challenges. Firstly, the required size of the second metasurface to collect all the beams becomes large, which compounds fabrication challenges. Secondly, the more rapid divergence at larger angles introduces an offset between the incident position of the chief ray on the metasurface and the corresponding focal spot, thereby introducing distortion<sup>17,36</sup>. This effect can be mitigated by using a non-air spacer of appropriate refractive index, as we have done here using fused silica ( $n = 1.46$ ) and BK7 glass ( $n = 1.52$ ). To reduce the weight of the optical system while maintaining similar optical performance, these spacers could be replaced by a lighter polymer of similar refractive index, for example, PMMA ( $n = 1.49$ <sup>37</sup>).

In this work, the aperture of the meta-optics is practically limited by the feasible write time using electron beam lithography. Other fabrication techniques, including deep ultraviolet (DUV) and nanoimprint lithography, provide much faster write time and are therefore more suitable for large apertures and mass production. Recent works have demonstrated scalable manufacturing of metalenses<sup>38–40</sup> and other metasurfaces<sup>41–44</sup> using these techniques. Furthermore, nanoimprinting can potentially be used to commercialize this meta-optic at a price comparable to that of existing optical systems. In the Supplementary Information, we detail efforts to develop scalable, large-aperture eyepiece meta-optics using DUV lithography. However, the resolution achieved in our DUV facilities is around 250 nm, which is insufficient to fabricate the designed meta-atoms operating in visible with sub-wavelength periodicity. We overcome this issue by utilizing larger periodicity meta-atoms but note that high-throughput argon fluoride photolithography has been used to pattern meta-optics with 280 nm periodicity<sup>45</sup> and therefore propose that this lithography technique could be used without compromising the meta-

atoms. We designed meta-atoms with 1100 nm periodicity and fabricated the full 2 cm aperture meta-optics using DUV lithography. However, a consequence of larger meta-atom periodicity is reduced phase sampling which has more pronounced effects for wide-angle meta-optics<sup>46</sup>. In this case, due to aliasing issues introduced by insufficient phase sampling, the field of view of these meta-optics is limited to approximately 40°. Details of the DUV fabrication and experiment results are included in the Supplementary Information.

We note that the presented meta-optic doublet is designed for single-wavelength illumination at 633 nm. This makes it immediately suitable for monochromatic applications such as night vision, while more work is required for extension to applications requiring full color. Much progress has been made in recent years to develop meta-optics with broadband operation in the visible regime<sup>18–20,47</sup>, but the simultaneous achievement of broadband operation and wide field of view has yet to be demonstrated. For single-layer meta-optics, there are fundamental tradeoffs between device thickness, NA, and bandwidth<sup>48</sup>. When extending this system to broadband operation, however, these limitations may be circumvented using a doublet configuration to provide additional degrees of freedom. In addition, high resolution over the entire field of view is not required due to the foveated nature of the human eye<sup>3,49,50</sup>; that is, performance requirements at the ultrawide field of view are relaxed, which may enable the extension of the design presented here to broadband applications. We emphasize that some of the recent inverse-designed meta-optics for full-color imaging already have sufficient contrast at vision-relevant spatial frequencies, albeit the field of view remains limited<sup>19,51</sup>.

In conclusion, we demonstrated a large aperture, wide field of view meta-optic doublet eyepiece for near-eye display applications. Our design considers realistic constraints such as eye relief, pupil size, and display size. In incremental steps towards a large aperture meta-optic eyepiece, we designed a smaller system with 1 cm entrance aperture as a proof of concept as well as a full-scale 2 cm entrance aperture system. In both cases, the experimental performance of the system closely agrees with the design and exhibits consistent performance over at least 60° full field of view. These findings represent promising results for the integration of meta-optics into full-scale near-eye display systems, including AR/VR and night vision.

## Materials and Methods

### Metasurface fabrication

The meta-optics are fabricated in a silicon nitride layer on quartz substrate (500  $\mu\text{m}$  thick). First, 750 nm SiN was deposited on the substrate via plasma-enhanced chemical

vapor deposition (Oxford; Plasma Lab 100). The sample was coated with electron beam photoresist (ZEP-520A) and patterned using electron beam lithography (JEOL; JBX6300FS). Afterwards, we deposited 80 nm alumina ( $\text{Al}_2\text{O}_3$ ) using an electron beam evaporator (CHA; SEC-600) and did liftoff with 1-methyl-2-pyrrolidionone to form a hard mask for etching. The silicon nitride was then etched in an inductively coupled plasma etcher (Oxford; PlasmaLab 100, ICP-180) using fluorine-based gas chemistry.

### Meta-optics characterization

The PSF of the meta-optics was measured on a home-built setup. The illumination source was a HeNe laser (Newport N-LHP-131) at 632.8 nm wavelength with 1400 MHz linewidth (FWHM). The laser output was coupled to a single-mode fiber with approximately 300 nm diameter fiber core. A refractive lens was used to collimate the output. For measurements at various angles of incidence, the fiber output and collimator unit were mounted on a rotating arm to provide smooth rotation up to  $40^\circ$ . An iris placed at the axis of rotation served as the pupil aperture. Each meta-optic was mounted on 3-axis translation stage for precise alignment. The focal spot was magnified via microscope objective (Nikon Plan Fluorite 20x, NA = 0.50, WD = 2.1 mm) followed by a tube lens. The output was measured on a GT1930C camera sensor with  $5.86 \mu\text{m}$  per pixel resolution. The effective pixel resolution given the relay optics was calibrated by imaging an object of known size with the relay system. For the data shown in Fig. 4a, c, the exposure time was  $83 \mu\text{s}$ , and for the data shown in Fig. 4b, d, the exposure time was  $69 \mu\text{s}$ . The camera and relay optics were mounted on a two-axis stage for precise positioning of focal length and lateral translation to collect off-axis PSFs. Schematics and further details of the PSF characterization setup are available in the Supplementary Information.

The experimental MTFs, shown in Fig. 4e, f, were calculated from the corresponding normalized PSFs shown in Fig. 4a, b. First, to correct for nonzero background value, an estimate of the mean background value was obtained from a  $200 \times 200$  pixel area near the corner of each image. This background value was then subtracted from the data. To calculate the MTF, we computed the 2D Fourier transform of the normalized and background-corrected PSF and took a line cut along the same axis as shown PSF cuts. The MTF was then converted from the spatial unit of lp/mm to the angular unit of cyc/mrad using the effective focal length, which is 5.84 mm for the 1 cm optics and 15.17 mm for the 2 cm optics.

For an imaging demonstration, we built an eye model consisting of a refractive lens of 2.5 mm focal length and a camera to collect the image, and both were mounted on the rotating arm. The meta-optics were mounted and

aligned according to the design. For the imaging object, the desired pattern was displayed on a micro-LED screen and a narrowband filter (Thorlabs FL632.8-1, FWHM  $\approx 1$  nm) was used to filter illumination to the desired wavelength. The microscope objective was used to re-image the display object to a lateral size of approximately 3 mm. To measure across the entire FoV, the display, filter, and objective were translated laterally to cover the designed 8 mm display size corresponding to  $40^\circ$  FoV. Further details of the experiment setup, including schematic diagrams and the meta-optic alignment procedure, are available in the Supplementary Information.

### Acknowledgements

We gratefully acknowledge assistance from the staff at UCSB Nanofabrication Facility for DUV Stepper lithography and etching. Biljana Stamenic ran all the lithography optimizations, SEM's, etch calibrations and final product wafers. Demis D. John provided fabrication process direction, developed the initial process and updated process to use  $\text{SiO}_2$ -hardmasked Ru etching, and mask design reviews. William J. Mitchell developed the Ruthenium hard mask process, and provided recipes and process input on how to deposit and etch both the Ru and  $\text{SiO}_2$  using his established processes. The lithography masks were purchased from Digidat, Inc. We gratefully acknowledge fabrication assistance from several individuals at the University of Washington. Erik Petersen deposited SiN and prepared wafers for future fabrication steps, and Arnab Manna for diced the completed wafers after DUV stepper fabrication. In addition, we acknowledge Tina Teichmann for assisting with the experimental measurements.

### Author details

<sup>1</sup>Department of Physics, University of Washington, Seattle, WA, USA. <sup>2</sup>Department of Electrical and Computer Engineering, University of Washington, Seattle, WA, USA. <sup>3</sup>Department of Materials Science and Engineering, Massachusetts Institute of Technology, Cambridge, MA, USA. <sup>4</sup>Department of Electrical and Computer Engineering, University of Massachusetts, Lowell, MA, USA. <sup>5</sup>Department of Electrical and Computer Engineering, University of California, Santa Barbara, CA, USA

### Author contributions

T.G. designed the meta-optic doublet system and phase profiles in Zemax. F.Y., L.M., H.Z., and H.Z. contributed to modeling and discussion. A.W.-S. and J.F. designed the meta-atom libraries and made the GDS files. J.F. fabricated the meta-optics. Q.T. and Z.H. assisted with developing the fabrication processes. A.W.-S., J.F., and Z.Z. conducted the experimental measurements. A.W.-S. and J.F. analyzed the experiment data. A.W.-S. and J.F. drafted the manuscript. For DUV Stepper lithography and etching, D.J. directed the fabrication process and B.S. ran all lithography optimizations, SEM's, and final product wafers. All authors contributed to the technical discussion and review of the manuscript. A.M., J.H., and T.G. supervised the project and coordinated the research.

### Funding

Funding for this work was supported by the DARPA-ENVision program. Part of this work was conducted at the Washington Nanofabrication Facility / Molecular Analysis Facility, a National Nanotechnology Coordinated Infrastructure (NNCI) site at the University of Washington with partial support from the National Science Foundation via awards NNCI-1542101 and NNCI-2025489. Part of this work was performed in the UCSB Nanofabrication Facility, an open-access laboratory.

### Data availability

Data underlying the results presented in this paper are not publicly available at this time but may be obtained from the authors upon reasonable request.

### Conflict of interest

A.M. is a co-founder of Tunoptix, which is commercializing similar meta-optics in the visible. T.G. and J.H. are co-founders of 2Pi Inc., a company commercializing metasurface optics.

**Supplementary information** The online version contains supplementary material available at <https://doi.org/10.1038/s41377-024-01674-0>.

Received: 24 June 2024 Revised: 25 September 2024 Accepted: 28 October 2024

Published online: 02 January 2025

## References

- Kress, B. C. Optical Architectures for Augmented-, Virtual-, and Mixed-Reality headsets. (Bellingham: SPIE Press, 2020).
- Xiong, J. H. Augmented reality and virtual reality displays: emerging technologies and future perspectives. *Light Sci. Appl.* **10**, 216 (2021).
- Chang, C. Toward the next-generation VR/AR optics: a review of holographic near-eye displays from a human-centric perspective. *Optica* **7**, 1563–1578 (2020).
- Shieh, K. K. & Lee, D. S. Preferred viewing distance and screen angle of electronic paper displays. *Appl. Ergon.* **38**, 601–608 (2007).
- Peli, E. Real vision & virtual reality. *Opt. Photonics N.* **6**, 28–34 (1995).
- Choi, M. H. et al. Recent applications of optical elements in augmented and virtual reality displays: a review. *ACS Appl. Opt. Mater.* **2**, 1247–1268 (2024).
- Waxman, A. M. et al. Solid-state color night vision: Fusion of low-light visible and thermal infrared imagery. *Linc. Lab. J.* **11**, 41–60 (1998).
- Cakmakci, O. et al. Holographic pancake optics for thin and light-weight optical see-through augmented reality. *Opt. Express* **29**, 35206–35215 (2021).
- Gao, Q. K. et al. Compact see-through 3d head-mounted display based on wavefront modulation with holographic grating filter. *Opt. Express* **25**, 8412–8424 (2017).
- Gopakumar, M. et al. Full-colour 3D holographic augmented-reality displays with metasurface waveguides. *Nature* **629**, 791–797 (2024).
- Jang, C. et al. Waveguide holography for 3D augmented reality glasses. *Nat. Commun.* **15**, 66 (2024).
- Huang, H. Q. et al. Leaky-wave metasurfaces for integrated photonics. *Nat. Nanotechnol.* **18**, 580–588 (2023).
- Chen, E. G. et al. Broadband beam collimation metasurface for full-color micro-LED displays. *Opt. Express* **32**, 10252–10264 (2024).
- Martins, A. et al. On metalenses with arbitrarily wide field of view. *ACS Photonics* **7**, 2073–2079 (2020).
- Shalaginov, M. Y. et al. Single-element diffraction-limited fisheye metalens. *Nano Lett.* **20**, 7429–7437 (2020).
- Arbabi, A. et al. Miniature optical planar camera based on a wide-angle metasurface doublet corrected for monochromatic aberrations. *Nat. Commun.* **7**, 13682 (2016).
- Yang, F. et al. Wide field-of-view metalens: a tutorial. *Adv. Photonics* **5**, 033001 (2023).
- Huang, L. et al. Full-color metaoptical imaging in visible light. *Adv. Photonics Res.* **3**, 2100265 (2022).
- Frösch, J. E. et al. Beating bandwidth limits for large aperture broadband nano-optics. Print at <https://doi.org/10.48550/arXiv.2402.06824> (2024).
- Tseng, E. et al. Neural nano-optics for high-quality thin lens imaging. *Nat. Commun.* **12**, 6493 (2021).
- Zhang, L. D. et al. High-efficiency, 80 mm aperture metalens telescope. *Nano Lett.* **23**, 51–57 (2023).
- Li, Z. Y. et al. Meta-optics achieves RGB-achromatic focusing for virtual reality. *Sci. Adv.* **7** (2021).
- Li, Z. Y. et al. Inverse design enables large-scale high-performance meta-optics reshaping virtual reality. *Nat. Commun.* **13**, 2409 (2022).
- Lee, G. Y. et al. Metasurface eyepiece for augmented reality. *Nat. Commun.* **9**, 4562 (2018).
- Chen, W. T. et al. Flat optics with dispersion-engineered metasurfaces. *Nat. Rev. Mater.* **5**, 604–620 (2020).
- Bayati, E. et al. Design of achromatic augmented reality visors based on composite metasurfaces. *Appl. Opt.* **60**, 844–850 (2021).
- Groever, B. et al. Meta-lens doublet in the visible region. *Nano Lett.* **8**, 4902–4907 (2017).
- Lohmann, A. W. Scaling laws for lens systems. *Appl. Opt.* **28**, 4996–4998 (1989).
- Martins, A. et al. Fundamental limits and design principles of doublet metalenses. *Nanophotonics* **11**, 1187–1194 (2022).
- Luke, K. et al. Broadband mid-infrared frequency comb generation in a Si<sub>3</sub>N<sub>4</sub> microresonator. *Opt. Lett.* **40**, 4823–4826 (2015).
- Malitson, I. H. Interspecimen comparison of the refractive index of fused silica. *J. Opt. Soc. Am.* **55**, 1205–1209 (1965).
- Liu, V. & Fan, S. S. A free electromagnetic solver for layered periodic structures. *Comput. Phys. Commun.* **183**, 2233–2244 (2012).
- Kress, B. & Starner, T. A review of head-mounted displays (HMD) technologies and applications for consumer electronics. Proceedings of SPIE 8720, Photonic Applications for Aerospace, Commercial, and Harsh Environments IV. Baltimore: SPIE, 2013, 87200A.
- Li, S. Y. & Hsu, C. W. Thickness bound for nonlocal wide-field-of-view metalenses. *Light Sci. Appl.* **11**, 338 (2022).
- Miller, D. A. B. Why optics needs thickness. *Science* **379**, 41–45 (2023).
- Lin, H. I. et al. Wide-field-of-view, large-area long-wave infrared silicon metalenses. *ACS Photonics* **11**, 1943–1949 (2024).
- Zhang, X. N. et al. Complex refractive indices measurements of polymers in visible and near-infrared bands. *Appl. Opt.* **59**, 2337–2344 (2020).
- Kim, J. et al. Scalable manufacturing of high-index atomic layer-polymer hybrid metasurfaces for metaphotonics in the visible. *Nat. Mater.* **22**, 474–481 (2023).
- Kim, J. et al. One-step printable platform for high-efficiency metasurfaces down to the deep-ultraviolet region. *Light Sci. Appl.* **12**, 68 (2023).
- Park, J. S. et al. All-glass 100 mm diameter visible metalens for imaging the cosmos. *ACS Nano* **18**, 3187–3198 (2024).
- Kim, J. et al. A water-soluble label for food products prevents packaging waste and counterfeiting. *Nat. Food* **5**, 293–300 (2024).
- Tao, J. et al. Mass-manufactured beam-steering metasurfaces for high-speed full-duplex optical wireless-broadcasting communications. *Adv. Mater.* **34**, 2106080 (2022).
- Kim, J. et al. Dynamic hyperspectral holography enabled by inverse-designed metasurfaces with oblique helicoidal cholesterics. *Adv. Mater.* **36**, 2311785 (2024).
- Kim, J. et al. Metasurface holography reaching the highest efficiency limit in the visible via one-step nanoparticle-embedded-resin printing. *Laser Photonics Rev.* **16**, 2200098 (2022).
- Kim, J. et al. 8" wafer-scale, centimeter-sized, high-efficiency metalenses in the ultraviolet. *Mater. Today* **73**, 9–15 (2024).
- Kim, S. et al. Anti-aliased metasurfaces beyond the Nyquist limit. Print at <https://doi.org/10.48550/arXiv.2406.11261> (2024).
- Shrestha, S. et al. Broadband achromatic dielectric metalenses. *Light Sci. Appl.* **7**, 85 (2018).
- Presutti, F. & Monticone, F. Focusing on bandwidth: achromatic metalens limits. *Optica* **7**, 624–631 (2020).
- Curcio, C. A. et al. Human photoreceptor topography. *J. Comp. Neurol.* **292**, 497–523 (1990).
- Saragadam, V. et al. Foveated thermal computational imaging prototype using all-silicon meta-optics. *Optica* **11**, 18–25 (2024).
- Frösch, J. E. et al. Real time full-color imaging in a meta-optical fiber endoscope. *eLight* **3**, 13 (2023).